Journal of Biomedical Optics

BiomedicalOptics.SPIEDigitalLibrary.org

Study of tissue oxygen supply rate in a macroscopic photodynamic therapy singlet oxygen model

Timothy C. Zhu
Baochang Liu
Rozhin Penjweini

SPIE.

Study of tissue oxygen supply rate in a macroscopic photodynamic therapy singlet oxygen model

Timothy C. Zhu,* Baochang Liu, and Rozhin Penjweini
University of Pennsylvania, School of Medicine, Department of Radiation Oncology, Philadelphia, Pennsylvania 19104, United States

Abstract. An appropriate expression for the oxygen supply rate (Γ_s) is required for the macroscopic modeling of the complex mechanisms of photodynamic therapy (PDT). It is unrealistic to model the actual heterogeneous tumor microvascular networks coupled with the PDT processes because of the large computational requirement. In this study, a theoretical microscopic model based on uniformly distributed Krogh cylinders is used to calculate $\Gamma_s = g\,(1 - [^3O_2]/[^3O_2]_0)$ that can replace the complex modeling of blood vasculature while maintaining a reasonable resemblance to reality; g is the maximum oxygen supply rate and $[^3O_2]/[^3O_2]_0$ is the volume-average tissue oxygen concentration normalized to its value prior to PDT. The model incorporates kinetic equations of oxygen diffusion and convection within capillaries and oxygen saturation from oxyhemoglobin. Oxygen supply to the tissue is via diffusion from the uniformly distributed blood vessels. Oxygen can also diffuse along the radius and the longitudinal axis of the cylinder within tissue. The relations of Γ_s to $[^3O_2]/[^3O_2]_0$ are examined for a biologically reasonable range of the physiological parameters for the microvasculature and several light fluence rates (ϕ). The results show a linear relationship between Γ_s and $[^3O_2]/[^3O_2]_0$, independent of ϕ and photochemical parameters; the obtained g ranges from 0.4 to 1390 μM/s. © 2015 Society of Photo-Optical Instrumentation Engineers (SPIE)
[DOI: 10.1117/1.JBO.20.3.038001]

Keywords: singlet oxygen dosimetry; photodynamic therapy; oxygen diffusion; microscopic model; macroscopic model.

Paper 140840R received Dec. 16, 2014; accepted for publication Feb. 4, 2015; published online Mar. 4, 2015.

1 Introduction

Photodynamic therapy (PDT) is a photochemical treatment modality used to treat malignant and nonmalignant conditions.[1] It is generally believed that the therapeutic effect in PDT is mainly attributed to the production of singlet oxygen ($^1O_2$), which involves the interaction of light, photosensitizer (PS), and ground-state oxygen ($^3O_2$) in the target tissue.[1] To evaluate the efficacy in generating $^1O_2$, direct monitoring of $^1O_2$ *in vivo* via singlet oxygen luminescence (SOL) at 1270 nm is preferable, but also technically challenging because of the short lifetime of $^1O_2$ in real biological environments.[2–4] Hence, the progress in transferring this direct approach to the clinic has not been significant in the past decade since the successful *in vivo* detection of SOL in 2002.[5] Alternatively, explicit measurements of one or all three components in PDT are more feasible although an ideal approach still requires continuous measurements during PDT. Studies have been conducted to investigate the effects of light [including total delivered light fluence and fluence rate (ϕ)] and PS concentration on PDT efficacy both *in vitro* and *in vivo* (PDT dosimetry).[1,6–13] The effect of oxygenation is much more easily examined in the *in vitro* model,[14] because it is relatively difficult to monitor and quantify the spatial distribution of oxygen continuously and noninvasively in a real biological system.

To completely characterize the PDT treatment outcomes and interpret experimental results, mathematical modeling of the complex PDT mechanisms and the production of $^1O_2$ are suggested.[13] The basic mathematical descriptions of the photochemical and photophysical reactions during PDT can then be adopted into an *in vitro* and/or *in vivo* biological environment to calculate the temporal and spatial distributions of PDT components (PS, $^3O_2$ and $^1O_2$ concentrations and ϕ).[13,15–17] A macroscopic PDT model was developed to extract the so-called reacted singlet oxygen $[(^1O_2)_{rx}]$ threshold dose at tumor tissue necrotic distances by fitting the calculated $^1O_2$ profile to measured necrosis induced by interstitial PDT.[13] This model considers light diffusion and a set of PDT kinetics equations incorporating the oxygen consumption rate per ϕ and PS concentration (ξ), the probability ratio of an $^1O_2$ molecule reacting with ground-state PS compared to the $^1O_2$ molecule reacting with a cellular target (σ), and the ratio of the monomolecular decay rate of the triplet state (T) PS to the bimolecular rate of the triplet PS quenching by $^3O_2$ (β), which can be potentially used as clinically practical dosimetry quantities. In this macroscopic model, the molecular oxygen supply rate to the target tissue was hypothesized as a linear function of fractional $^3O_2$ concentration (the ratio of volume average oxygen concentration to its initial value prior to PDT) with a maximum supply rate (g), as shown in Eq. (1).

$$\Gamma_s = g\left[1 - \frac{[^3O_2]}{[^3O_2](t=0)}\right]. \tag{1}$$

Preliminary results were presented on fitting the necrotic radius induced by interstitial Photofrin-mediated PDT to obtain model parameters (ξ, σ, β, and g) and $[^1O_2]_{rx}$. Then, the sensitivity of the model parameters to calculated $[^1O_2]_{rx}$ profiles has been explored for different light source geometries and PSs in *in vivo* interstitial conditions.[13] A comparison of the

*Address all correspondence to: Timothy C. Zhu, tzhu@mail.med.upenn.edu

1083-3668/2015/$25.00 © 2015 SPIE

computed $[^1O_2]_{rx}$ distributions showed that the model can be potentially correlated to differences in PDT efficacy.

In the current study, a microscopic model incorporating biological blood vasculature distribution is used to investigate an appropriate simple expression for oxygen supply which can be used in our macroscopic model. Due to the large computational requirement, modeling of the heterogeneity of tumor microvascular networks coupled with the PDT processes is at present impractical. The ultimate objective of this study is to replace the complex modeling of blood vasculature with a simplified expression for oxygen supply to tissue while maintaining reasonable accuracy. The findings of the present studies justify that our previously hypothesized linear expression in the macroscopic PDT model is sufficient to replace microscopically modeling oxygen supply in tissue. The values of $g = 0.7 - 2.0\ \mu M/s$ as determined in the literature[13,18] for a number of PSs are also found to be within the range of g values calculated in this study for the range of the physiological parameters being tested.

2 Theory and Method

2.1 *Macroscopic Model for Photodynamic Therapy*

The macroscopic PDT model is briefly described in this section, as well as the definitions of the five parameters to be optimized during the process of fitting in the *in vivo* experimental results. The intention of this work is to investigate the oxygen supply term in the model using a microscopic model instead of fitting experimental results to derive parameters. More detailed descriptions of the model and the fitting routine can be found elsewhere.[13]

In the macroscopic model,[13] spatial distribution of ϕ in the tumor is calculated via Eq. (2) based on the diffusion approximation. Temporal and spatial distributions of PS (S_0), $[^3O_2]$ and $[^1O_2]$ concentrations are obtained by solving a set of coupled time-dependent differential Eqs. (3) to (5). The cumulative concentration of $[^1O_2]_{rx}$ can then be derived by the integration of Eq. (5) over time (t). In Eq. (4), the symbol Γ_s denotes the rates at which $^3O_2$ is supplied to the surrounding tissue, which is the term to be examined in this study.

$$\mu_a\phi - \nabla\cdot\left(\frac{1}{3\mu_s'}\nabla\phi\right) = S, \tag{2}$$

$$\frac{d[S_0]}{dt} + \left[\xi\sigma\frac{\phi([S_0]+\delta)[^3O_2]}{[^3O_2]+\beta}\right][S_0] = 0, \tag{3}$$

$$\frac{d[^3O_2]}{dt} + \left\{\xi\frac{\phi[S_0][1+\sigma([S_0+\delta])]}{[^3O_2]+\beta}\right\}[^3O_2] = \Gamma_s, \tag{4}$$

$$\frac{d[^1O_2]_{rx}}{dt} - f\cdot\left[\xi\frac{\phi([S_0][^3O_2])}{[^3O_2]+\beta}\right] = 0. \tag{5}$$

The parameters μ_s' and μ_a represent optical scattering and absorption coefficients, respectively. δ is the low concentration correction parameter and S describes the light source. The mathematical definitions of all parameters are given in Tables 1 and 2.

Table 1 Photodynamic therapy (PDT) photochemical parameters used for calculations for Photofrin.[13]

Parameters	Values	Definitions
ξ ($cm^2\,mW^{-1}\,s^{-1}$)	3.70×10^{-3}	$S_\Delta k_5/(k_3+k_5)\varepsilon/h\upsilon/(k_6/k_7[A]+1)$
σ (μM^{-1})	7.60×10^{-5}	$k_1/(k_7[A])$
δ (μM)	33.00	Low concentration correction
β (μM)	11.90	k_4/k_2
μ_s' (cm^{-1})	13.46	Optical reduced scattering coefficient
μ_a (cm^{-1})	1.03	Optical absorption coefficient

Some reported values of the photochemical parameters for Photofrin are shown in Table 1.[13]

2.2 *Microscopic Model for Photodynamic Therapy*

A microscopic PDT model was developed based on the Krogh cylinder model.[19] In the model, the tumor has uniformly spaced cylindrical blood capillaries (with a radius of R_c) in parallel with the linear light source. The inter-capillary distance between two adjacent capillaries is assumed to be large enough so that each capillary can supply oxygen only to its immediate concentric surrounding tissue. The oxygen concentration in the oxygen supply term as expressed in Eq. (1) will be an average value over the entire tissue element volume. Due to the values of both inter-capillary distance (R_t) and capillary length (l_z)

Table 2 Definitions of the photochemical parameters.

Symbols	Definitions	Units
k_1	Photobleaching rate	$1/\mu M\cdot s$
k_2	Reaction rate of $^3O_2$ with T	$1/\mu M\cdot s$
k_3	Rate of S_1 to S_0	1/s
k_4	Rate of T to S_0	1/s
k_5	Rate of S_1 to T	1/s
k_6	Rate of $^1O_2$ to $^3O_2$	1/s
k_7	React. rate of $^1O_2$ and tissue	$1/\mu M\cdot s$
ε	Extinction coefficient	$cm^{-1}\,\mu M^{-1}$
g	Maximum oxygen supply rate	$\mu M/s$
$[S_0]$	Ground state sensitizer concentration	μM
$[S_1]$	Singlet excited state sensitizer concentration	μM
$[T]$	Triplet excited state sensitizer concentration	μM
$[^3O_2]$	Triplet ground state oxygen concentration	μM
$[^1O_2]$	Singlet excited state oxygen concentration	μM
S_Δ	Fraction $[^1O_2]$ from $[T]$ and $[^3O_2]$ reaction	Dimensionless

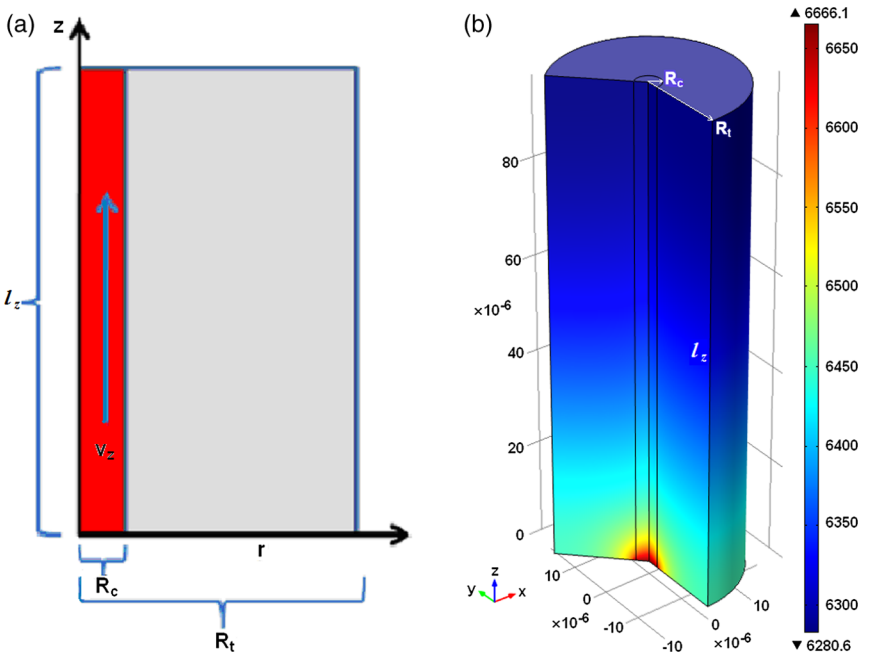

Fig. 1 (a) A schematic of the Krogh cylinder model. (b) three-dimensional (3-D) mesh plot of the Krogh cylinder model. The light fluence rate within the Krogh model is considered to be a constant because the spatial scale of light transport (~1 to 10 mm) is much larger than the spatial scale of the Krogh model (<0.4 mm = 400 μm). The incident direction of light is randomly distributed.

used in this study, it is reasonable to assume that ϕ within the small tissue element in Fig. 1 is constant. Figure 1 shows the schematic of the cylindrical Krogh model. Note that a three-dimensional Krogh model can be simplified as a 2-D cylindrical symmetric model given the above assumptions.

Before introducing the governing equations for oxygen and its carrier, oxyhemoglobin (HbO), some basic physiological assumptions are discussed first. Oxygen is normally present in the blood in two forms: chemically bound to hemoglobin forming HbO, and free molecules dissolved in the plasma. Most oxygen is bound to form HbO, which is contained in the red blood cell (RBC). However, there is still a small fraction of oxygen dissolved in the liquid media such as blood plasma and RBC water. The concentration of these free oxygen molecules can be represented using a quantity called oxygen partial pressure (P). The relation between them can be defined using Henry's law in Eq. (6), where α is the oxygen solubility coefficient:

$$[^3O_2] = \alpha P. \tag{6}$$

When P decreases in the surrounding environment, HbO will release oxygen and vice versa. The percentage of hemoglobin that is saturated with oxygen is usually referred to as hemoglobin oxygen saturation (SaO_2). The relationship between P and SaO_2 is described by Hill's oxygen dissociation curve. A mathematic expression for $^3O_2$ dissociation is Hill's equation, as shown in Eq. (7):[16]

$$\mathrm{Sa} = \frac{P^n}{P^n + P_{50}^n}, \tag{7}$$

where P_{50} represents the half maximum hemoglobin saturation pressure. n is the Hill coefficient representing the degree of cooperativity.

Oxygen molecules can diffuse freely from RBC into the blood stream due to negligible resistance in the membrane.[19] Therefore, the first assumption is that released oxygen from HbO can instantaneously be present in blood plasma (i.e., ignoring the diffusion from RBC). The second assumption is that RBCs are uniformly distributed in the blood.

Given the above assumptions, the time-dependent governing equations for $^3O_2$ and HbO transport inside the capillary are given in Eqs. (8) and (9). First, note that the concentration of $^3O_2$ is hereafter expressed using the partial pressure of $^3O_2$ (P) based on Eq. (6) because of the continuity boundary conditions that will be discussed later. Second, Sa in Eq. (9) is the hemoglobin oxygen saturation describing the percentage of HbO concentration to total hemoglobin concentration.

$$\alpha_c \frac{\partial P}{\partial t} = \alpha_c D_c \nabla^2 P - v \cdot \alpha_c \nabla P + \Gamma_{\mathrm{rec}}, \tag{8}$$

$$C_H \frac{\partial \mathrm{Sa}}{\partial t} = C_H D_H \nabla^2 \mathrm{Sa} - v \cdot C_H \nabla \mathrm{Sa} - \Gamma_{\mathrm{rec}}. \tag{9}$$

The product of Sa and C_H (total hemoglobin concentration in capillary) is the HbO concentration. The first terms on the right hand sides of Eqs. (8) and (9) are the diffusion terms of $^3O_2$ and hemoglobin, respectively; the second terms describe the convection processes. The third term (Γ_{rec}) is the so-called "reaction" term representing the $^3O_2$ loading/unloading from deoxyhemoglobin/oxyhemoglobin. The parameters D_c and D_H represent the diffusion coefficients of $^3O_2$ and hemoglobin in the capillary, respectively. α_c is the solubility of $^3O_2$ in plasma and v is the blood velocity in the capillary.

By manipulating Eqs. (7) to (9), one can derive the main governing Eq. (10) for P in the capillary, where K and M are defined in Eqs. (11) and (12), respectively.

$$(\alpha_c + KC_H)\frac{\partial P}{\partial t} = (\alpha_c D_c + KC_H D_H)\nabla^2 P - (\nu_z \alpha_c + \nu_z KC_H)\frac{\partial P}{\partial z} + C_H D_H M\left[\left(\frac{\partial P}{\partial r}\right)^2 + \left(\frac{\partial P}{\partial z}\right)^2\right], \quad (10)$$

$$K = \frac{nP^{n-1}P_{50}^n}{(P^n + P_{50}^n)^2}, \quad (11)$$

$$M = \frac{n(n-1)P_{50}^n P^{n-2}(P^n + P_{50}^n) - 2n^2 P^{(2n-2)}P_{50}^n}{(P^n + P_{50}^n)^3}, \quad (12)$$

where r and z are the radial and axial variables, respectively. v_z is the axial blood flow velocity.

The boundary conditions in the microscopic model are summarized in Eqs. (13) to (16). The bottom end of the capillary (i.e., $z = 0$) is the entrance of blood flow, which is assumed to have a constant $^3O_2$ partial pressure P_{ts}. On the boundary between capillary and tissue, both $^3O_2$ flux and P are continuous as shown in Eqs. (14) and (15). Other boundaries are considered as insulation.

$$P|_{z=0, r\in[0,R_c]} = P_{ts}, \quad (13)$$

$$D_c\alpha_c \nabla P|_{r=R_c^-} = D_t\alpha_t \nabla P|_{r=R_c^+}, \quad (14)$$

$$P|_{r=R_c^-} = P|_{r=R_c^+}, \quad (15)$$

$$\nabla P|_{other} = 0. \quad (16)$$

The parameters α_t and D_t are the solubility and diffusion coefficients of oxygen in tissue, respectively.

The governing equation for $[^3O_2]$ in tissue during PDT in the microscopic model is given by Eq. (17), which has the same terms on the left-hand side as Eq. (4) to describe PDT consumption of oxygen. The right-hand side of the equation contains both $^3O_2$ diffusion (the first term) and the metabolic consumption (the second term). However, only a general oxygen supply term Γ_s is used in the macroscopic model [as shown in Eq. (4)].

$$\frac{\partial[^3O_2]}{\partial t} + \left\{\xi\frac{\phi[S_0][^3O_2][1 + \sigma([S_0] + \delta)]}{[^3O_2] + \beta}\right\} = D_t\nabla^2[^3O_2] - q_0\frac{[^3O_2]}{[^3O_2] + \alpha_t P_m}. \quad (17)$$

The parameter q_0 represents the maximum metabolic $^3O_2$ consumption rate and P_m is the half-maximum oxygen consumption.

Table 3 presents the magnitude of the physiological parameters based on the literature values for the normal and tumor tissues by either measurements (in both living animals and fixed tissues) or theoretical studies.[16,19–25] The normal capillaries appear as fine, nearly parallel vessels that are served by orderly branching arterial and venous trees.[21] In contrast, the tumor vessels are disorganized, leaving large, irregular avascular spaces.[21] We tried to cover the existing wide range data sets representing both normal and cancer tissues in our study.

Table 3 Physiological parameters in the microscopic PDT model. The standard values are considered as the benchmark condition for the comparison.

Parameters	Ranges	Standard values	Description
R_t	18–60[19,20,21]	60	Radius of cylindrical tissue (μm)
R_c	2.5–10[19,20,21]	4	Radius of cylindrical capillary (μm)
D_t		1700[19]	$^3O_2$ diffusion coefficient in tissue ($\mu m^2/s$)
D_c		1240[24]	$^3O_2$ diffusion coefficient in capillary ($\mu m^2/s$)
α_t		1.295[19]	$^3O_2$ solubility in tissue (μM/mmHg)
α_c		1.527[19]	$^3O_2$ solubility in plasma (μM/mmHg)
v_z	50–200[19,24]	100[24]	Blood flow velocity (μm/s)
P_{50}		26[16]	Half maximum hemoglobin saturation pressure (mmHg)
C_H		2500[26,*]	Total hemoglobin concentration in capillary (μM)
q_0	0.9–6	2.4[19]	$^3O_2$ maximum metabolic consumption rate (μM/s)
n		2.46[24]	Hill constant
P_m		0.386[24]	pO_2 at half maximum oxygen consumption concentration (mmHg)
P_{ts}	50, 100[19,25,27]	100[25]	Artery $^3O_2$ partial pressure (mmHg)
D_H		14[19]	Hemoglobin diffusion coefficient in capillary ($\mu m^2/s$)
l_z	100–400[19,20]	220	Length of capillary (μm)

Note: * The hemoglobin concentration in a red blood cell is 5000 μM.[16] Thus the hemoglobin concentration is 2500 μM after we factor in the fraction of the red blood cell, ie. hematocrit, in blood is about 50%.[26]

2.3 *Simulation, Procedures, and Initial Conditions*

The microscopic model was simulated by the finite element method (FEM) analysis, solver, and simulation software package COMSOL Multiphysics v4.3b (Comsol AB, Stockholm, Sweden), which was run on an iMAC OSX version 10.9.5 (Processor 3.1 GHz Intel Core 17 and Memory 16 GB 1600 MHz DDR3). LiveLink for MATLAB® was also used

to work with COMSOL Multiphysics in combination with MATLAB R2013a (64-bit, Massachusetts).

The first step was to examine an expression for oxygen supply. For this purpose, the instantaneous total change rates of $^3O_2$ in tissue [i.e., the sum of the two terms on the right-hand side of Eq. (17)] were calculated, and then plotted as a function of the instantaneous oxygen concentration at the corresponding time normalized to its value prior to PDT ($[^3O_2]/[^3O_2]_0$). These simulations were first performed for a range of ϕ (25 to 150 mW/cm^2), and some typical treatment conditions for Photofrin-, mTHPC-, BPD-, and HPPH-mediated PDT. Different photochemical parameters ξ ($3.7\times10^{-3}-76\times10^{-3}$ cm^2 mW^{-1} s^{-1}), σ ($1.55\times10^{-5}-7.6\times10^{-5}$ μM^{-1}) and β (8.7 to 11.9 μM) were used in this step. The results were analyzed together to see the ϕ, ξ, σ, and β dependence.

The main objective of the second step was to find g values in Photofrin-mediated PDT for a range of physiological microenvironments at $\phi = 150$ mW/cm^2. The initial Photofrin concentration in the tissue was assumed to be 7 μM and total treatment time was chosen to be 100 min. The standard values of the PDT photochemical and physiological parameters, reported by the other studies, were used as shown in Tables 1 and 3.[16,19–25] The radius of the capillary ($R_c = 2.5$, 4.0 or 10 μm), the length of the capillary ($l_z = 100$, 220 or 400 μm), the density of blood vessels ($R_t = 18$, 30 or 60 μm), the blood flow velocity ($v_z = 50$, 100 or 200 μm/s), and maximum $^3O_2$ metabolic consumption rate ($q_0 = 0.9$, 2.4 or 6 μM/s) were set at three

Table 4 Physiological parameters varied for the range of microenvironment examined for g.

				g (μM/s)								
				R_c; R_t (μm)								
P_{ts} (mmHg)	q_0 (μM/s)	v_z (μm/s)	l_z (μm)	2.5;60	4;60	2.5;30	10;60	4;30	2.5;18	4;18	10;30	10;18
100	0.9	50	220	0.9	2.3	4.0	8.6	6.6	8.3	16.8	28.3	80.1
		100	220	2.0	4.4	7.0	17.2	14.9	15.5	29.1	51.9	147.0
		200	220	4.2	7.9	11.9	27.2	23.1	26.1	56.0	104.2	279.6
	2.4	50	220	0.9	2.1	4.1	10.6	8.8	9.1	18.5	28.8	82.7
		100	220	2.0	4.9	8.3	17.7	15.4	17.3	31.2	61.1	149.1
		200	220	3.9	7.9	13.9	36.4	30.6	31.7	87.2	104.9	282.7
	6	50	220	0.9	2.0	4.1	12.1	9.2	9.5	23.3	35.7	89.9
		100	220	2.0	4.9	9.2	20.0	15.9	18.2	33.2	68.7	155.7
		200	220	4.4	7.8	14.5	31.1	26.1	29.0	55.8	109.9	286.1
50	0.9	50	220	0.6	2.3	4.2	10.8	10.8	12.4	25.5	49.1	151.7
		100	220	1.9	4.6	8.2	18.8	18.7	23.0	44.0	93.8	297.5
		200	220	3.4	8.1	14.4	37.6	34.0	48.7	89.0	167.1	601.5
	2.4	50	220	0.9	2.2	3.9	10.8	11.3	14.5	27.4	51.2	152.2
		100	220	1.9	4.6	8.9	20.4	17.9	25.4	49.0	93.9	305.6
		200	220	3.4	7.5	15.2	37.7	30.8	45.7	88.2	167.2	604.6
	6	50	220	1.0	2.3	4.4	11.0	10.7	14.9	33.5	55.8	161.8
		100	220	1.9	4.6	7.4	20.7	16.0	25.8	52.2	94.3	325.5
		200	220	3.6	5.5	15.7	45.5	30.7	54.0	86.4	168.5	606.9
100	2.4	100	100	4.9	7.7	13.0	37.7	29.7	30.7	75.4	111.2	277.3
		100	220	2.0	4.9	8.3	17.7	15.4	17.3	31.2	61.1	149.1
		100	400	1.0	2.3	5.1	9.5	10.7	11.0	19.9	30.2	88.1
50	2.4	100	100	3.1	7.7	16.5	38.9	36.7	51.4	99.6	158.9	642.3
		100	220	1.9	4.6	8.9	20.4	17.9	25.4	49.0	93.9	305.6
		100	400	0.9	2.2	3.8	9.7	8.9	13.2	32.6	57.7	204.2

different values, which cover the existing data sets representing both normal and tumor vasculatures.[19–24] The magnitude of P_{ts} was set at two different values of 50 and 100 mmHg representing $^3O_2$ partial pressure in both tumor and normal arteries.[19,22–25,27] For the simulations, the physiological parameters were first set at their standard values and then the magnitude of R_c, R_t, v_z, q_0, P_{ts} and l_z were varied from their standard values. The varied parameters with their values are listed in Table 4 along with the fitted results in the next section.

3 Results and Discussions

3.1 *Linear Correlation and g Calculation for Different Photochemical Parameters and Fluence Rates in a Capillary with Standard Physiological Parameters*

Figures 2(a) and 2(b) show the volume-averaged oxygen supply rate and $^3O_2$ concentration over the whole Krogh cylinder as a function of time, calculated using the microscopic model for standard values presented in Table 3 and $\phi = 25$, 50, 75, 100, and 150 mW/cm^2. Based on our calculations, the initial volume-averaged oxygen concentration $[^3O_2]_0$, prior to Photofrin-mediated PDT (with $\xi = 3.7 \times 10^{-3}$ cm^2 mW^{-1} s^{-1}, $\sigma = 7.6 \times 10^{-5}$ μM^{-1}, $\beta = 11.9$ μM, $\delta = 33$ μM), was around 39.41 μM. The corresponding volume-averaged oxygen supply rate versus $[^3O_2]/[^3O_2]_0$ is presented in Fig. 2(c), which is "zero" prior to PDT and shows a linear correlation independent of ϕ. A linear fit to these data (has an intercept at 1 on x-axis) results in a slope of about 4.9 ± 0.1, which represents the g value in μM/s with the standard deviation of the mean (STDM). The simulations were also performed for different PSs: mTHPC (with $\xi = 30 \times 10^{-3}$ cm^2 mW^{-1} s^{-1}, $\sigma = 2.97 \times 10^{-5}$ μM^{-1}, $\beta = 8.7$ μM, $\delta = 33$ μM), BPD (with $\xi = 51 \times 10^{-3}$ cm^2 mW^{-1} s^{-1}, $\sigma = 1.7 \times 10^{-5}$ μM^{-1}, $\beta = 11.9$ μM, $\delta = 33$ μM) and HPPH (with $\xi = 76 \times 10^{-3}$ cm^2 mW^{-1} s^{-1}, $\sigma = 1.55 \times 10^{-5}$ μM^{-1}, $\beta = 11.9$ μM, $\delta = 33$ μM) at $\phi = 150$ mW/cm^2. The volume-averaged oxygen supply rate versus $[^3O_2]/[^3O_2]_0$ is presented in Fig. 2(d) and shows a linear correlation independent of ξ, σ and β. The linear fit to these data results in a g value of about 5.1 ± 0.2 μM/s (g is presented with

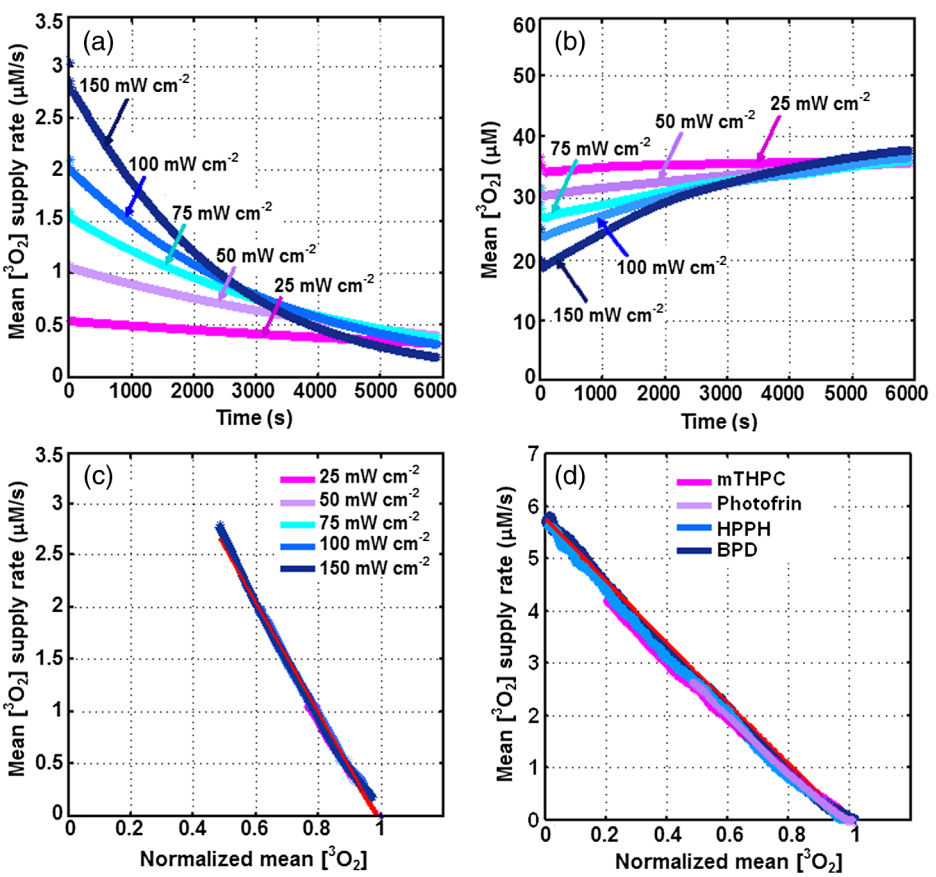

Fig. 2 (a) Oxygen supply rate [right-hand side of Eq. (17)] and (b) oxygen concentration, defined as the volumetric average around each vessel versus time. The plots are for $\phi = 25$, 50, 75, 100, and 150 mW cm^{-2}. (c) The mean oxygen supply rate versus normalized mean oxygen for different ϕ. A linear fit to the spectra (as shown with red lines) results an average slope of about 4.99 ± 0.10, which is $g(\mu M/s) \pm$ STDM. (d) The mean oxygen supply rate versus normalized oxygen for different photosensitizers (PSs), Photofrin ($\xi = 3.7 \times 10^{-3}$ cm^2 mW^{-1} s^{-1}, $\sigma = 7.6 \times 10^{-5}$ μM^{-1}, $\beta = 11.9$ μM, $\delta = 33$ μM), mTHPC ($\xi = 30 \times 10^{-3}$ cm^2 mW^{-1} s^{-1}, $\sigma = 2.97 \times 10^{-5}$ μM^{-1}, $\beta = 8.7$ μM, $\delta = 33$ μM), BPD ($\xi = 51 \times 10^{-3}$ cm^2 mW^{-1} s^{-1}, $\sigma = 1.7 \times 10^{-5}$ μM^{-1}, $\beta = 11.9$ μM, $\delta = 33$ μM) and HPPH ($\xi = 76 \times 10^{-3}$ cm^2 mW^{-1} s^{-1}, $\sigma = 1.55 \times 10^{-5}$ μM^{-1}, $\beta = 11.9$ μM, $\delta = 33$ μM). A linear fit to the spectra (as shown with red lines) results $g = 5.12 \pm 0.17$ μM/s. The data are plotted for the physiological parameters with standard values presented in Table 3. Normalized mean oxygen is defined as the volumetric average of $^3O_2$ around each vessel divided by $[^3O_2]_0$, which is the initial mean oxygen before PDT.

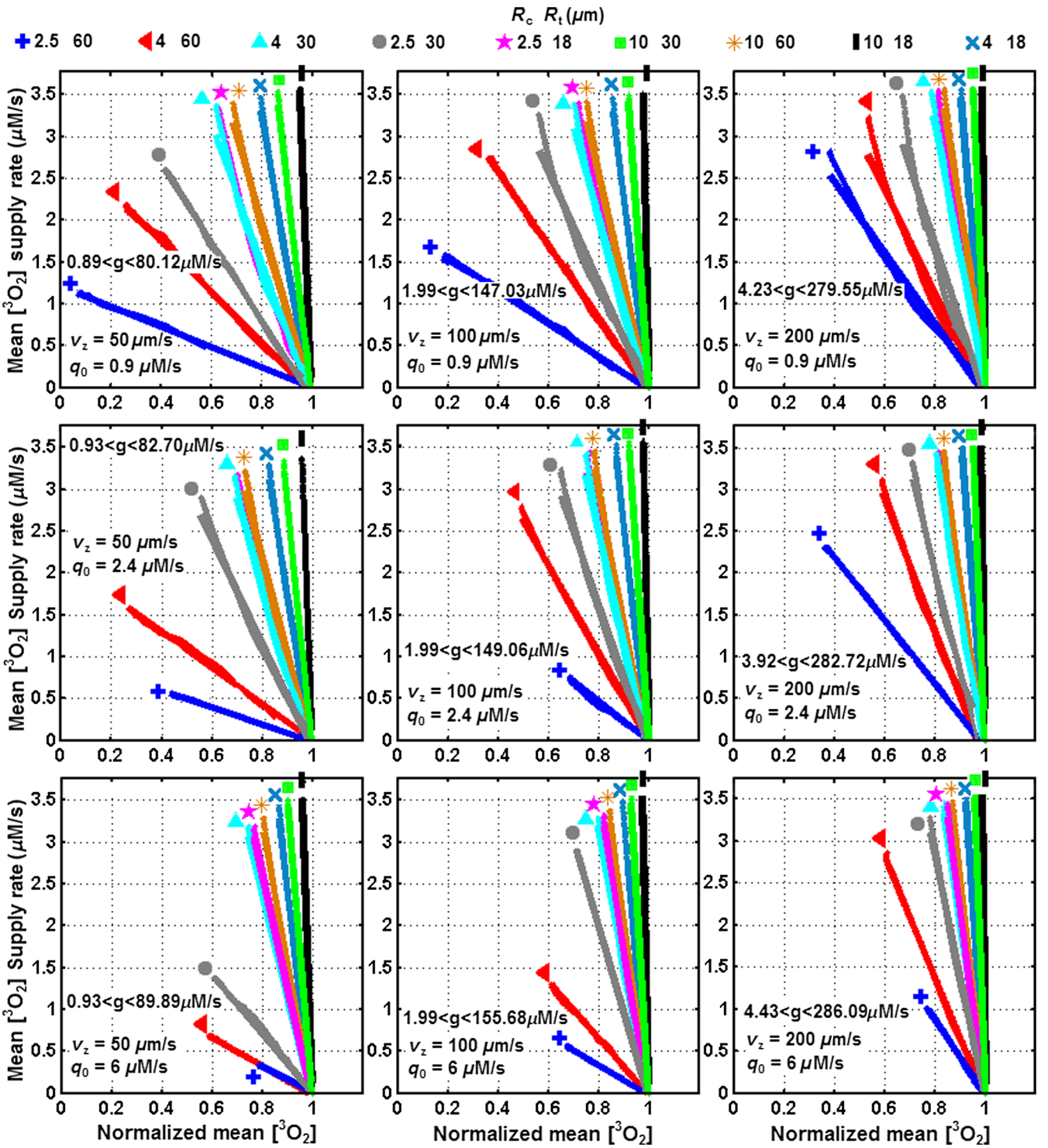

Fig. 3 Calculated mean oxygen supply rate [right side of Eq. 17] versus normalized mean oxygen, $[^3O_2]/[^3O_2]_0$. The data are plotted for artery oxygen partial pressure $P_{ts} = 100$ mmHg, capillary length $l_z = 220$ μm as well as different blood flow v_z and maximum metabolic oxygen consumption rate q_0. Each plot contains nine combinations of cylindrical tissue radius R_t (18, 30, 60 μm) and capillary radius R_c (2.5, 4, 10 μm) as presented with different colors and symbols. The 3 plots for the left column are for $v_z = 50$ μm/s and $q_0 = 0.9$, 2.4, and 6 μM/s, respectively; the 3 plots for the middle column are for $v_z = 100$ μm/s and $q_0 = 0.9$, 2.4, and 6 μM/s, respectively; the 3 plots for the right column are for $v_z = 200$ μm/s and $q_0 = 0.9$, 2.4, and 6 μM/s, respectively. The calculated g values are in the range of 0.89–286.09 μM/s.

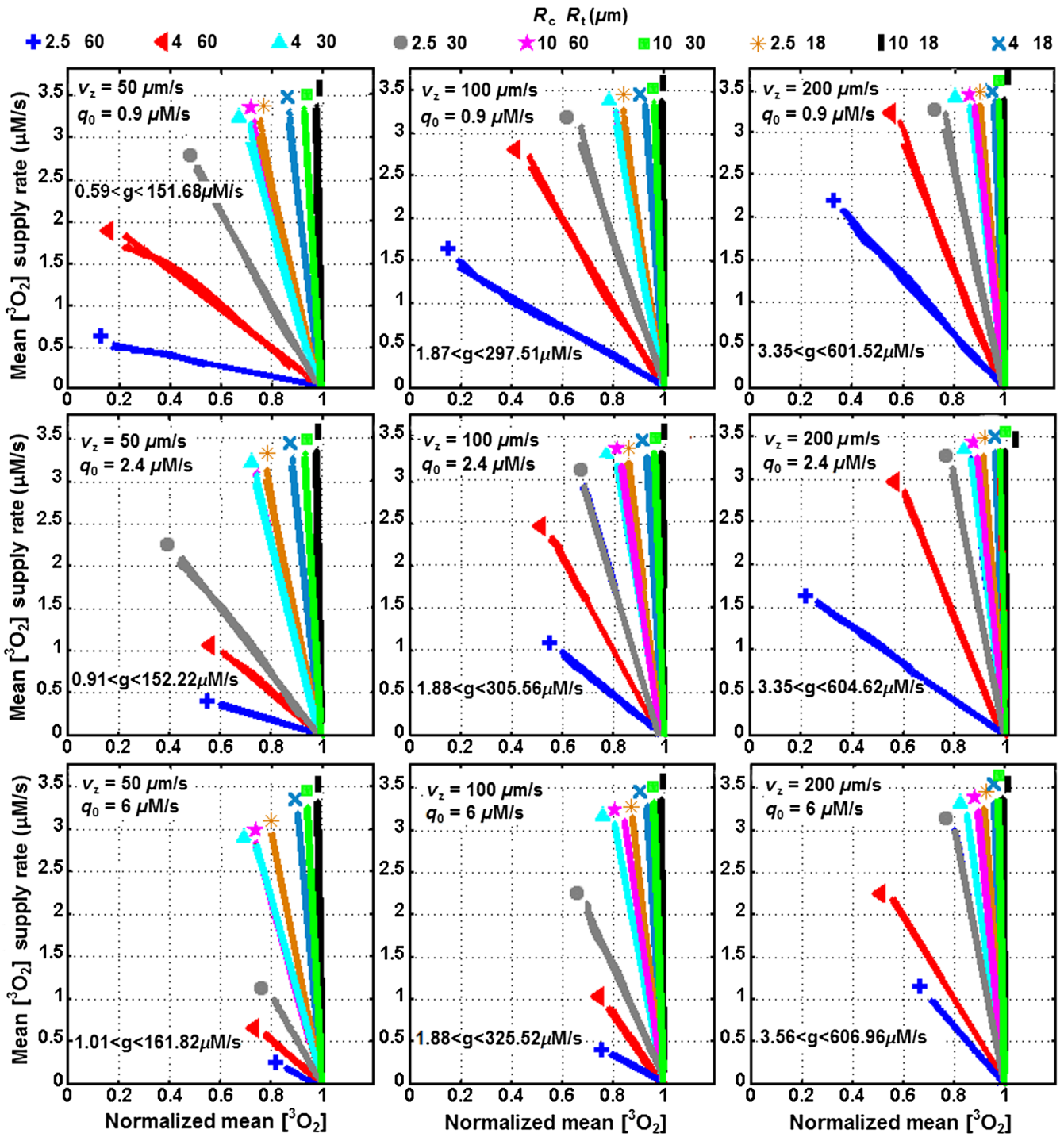

Fig. 4 Calculated mean oxygen supply rate [right side of Eq. 17] versus normalized mean oxygen, $[^3O_2]/[^3O_2]_0$. The data are plotted for artery oxygen partial pressure $P_{ts} = 50$ mmHg, capillary length $l_z = 220$ μm as well as different blood flow v_z and maximum metabolic oxygen consumption rate q_0. Each plot contains nine combinations of cylindrical tissue radius R_t (18, 30, 60 μm) and capillary radius R_c (2.5, 4, 10 μm) as presented with different colors and symbols. The 3 plots for the left column are for $v_z = 50$ μm/s and $q_0 = 0.9$, 2.4, and 6 μM/s, respectively; the 3 plots for the middle column are for $v_z = 100$ μm/s and $q_0 = 0.9$, 2.4, and 6 μM/s, respectively; the 3 plots for the right column are for $v_z = 200$ μm/s and $q_0 = 0.9$, 2.4, and 6 μM/s, respectively. The calculated g values are in the range of 0.59–606.96 μM/s.

STDM). While the g value is extremely sensitive to change in the physiological parameters and $^3O_2$ concentration, the results show that g is independent of ϕ and PS photochemical parameters.

3.2 *Representative g Value Tests on More Than One Varying Parameter*

The g values were calculated for Photofrin-mediated PDT and a range of physiological parameters at $\phi = 150$ mW/cm^2. In our model, the blood vessel network forms uniformly distributed Krogh cylinders and the spacing between vascular cylinders R_t varies between 18 and 60 μm. The cylindrical blood capillary has R_c in the range of 2.5 to 10 μm and l_z in the range of 100 to 400 μm. For both tumor and normal vasculatures, the maximum $^3O_2$ metabolic consumption rate (q_0) and blood velocity in capillary (v_z) are in the ranges of 0.9 to 6 μM/s and 50 to 200 μm/s, respectively (see Table 3).

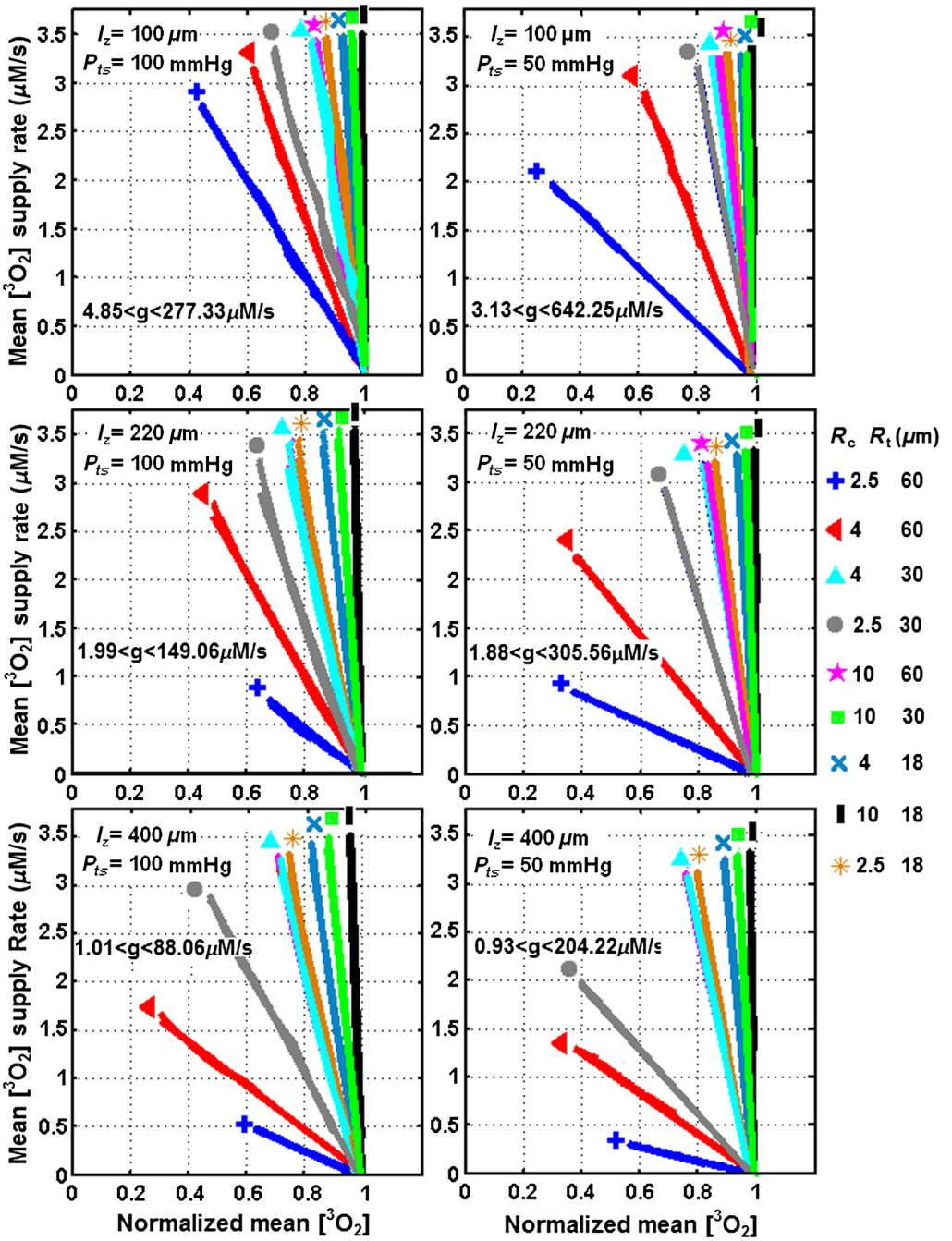

Fig. 5 Calculated mean oxygen supply rate [right side of Eq. 17] versus normalized mean oxygen, $[^3O_2]/[^3O_2]_0$. The data are plotted for blood flow $v_z = 100$ μm/s, maximum metabolic oxygen consumption rate $q_0 = 2.4$ μM/s as well as different artery oxygen partial pressure P_{ts} and capillary length l_z. Each plot contains 9 combinations of cylindrical tissue radius R_t (18, 30, 60 μm) and capillary radius R_c (2.5, 4, 10 μm) as shown with different colors and symbols. The 3 plots for the left column are for $P_{ts} =$ 100 mmHg and $l_z = 100, 220,$ and 400 μm, respectively; the 3 plots for the right column are for $P_{ts} = 50$ mmHg and $l_z = 100, 220,$ and 400 μm, respectively. The g values are in the ranges of 1.01–277.33 μM/s and 0.93–642.25 μM/s for $P_{ts} = 100$ and 50 mmHg, respectively.

The oxygen pressure at the aortal entrance of the blood vessel (P_{ts}) is assumed to be in the range of 50 or 100 mmHg.[19,25,27] The linear correlation between the volume-averaged oxygen supply rate and $[^3O_2]/[^3O_2]_0$ as well as their respective g values is presented in Figs. 3 to 5 and Table 4. The linear fits to the data result in g values in the ranges of 0.9 to 286.1 μM/s for $P_{ts} = 100$ mmHg and $0.6 - 606.9$ μM/s for $P_{ts} = 50$ mmHg.

3.3 *Formulation of g Directly from Blood Vessel Physiological Parameters*

The convective oxygen delivery (Q) is related to the product of blood flow ($v_z \pi R_c^2$) and oxygen concentration by Fick's principle:[28]

$$Q = \pi R_c^2 v_z [^3O_2]. \tag{18}$$

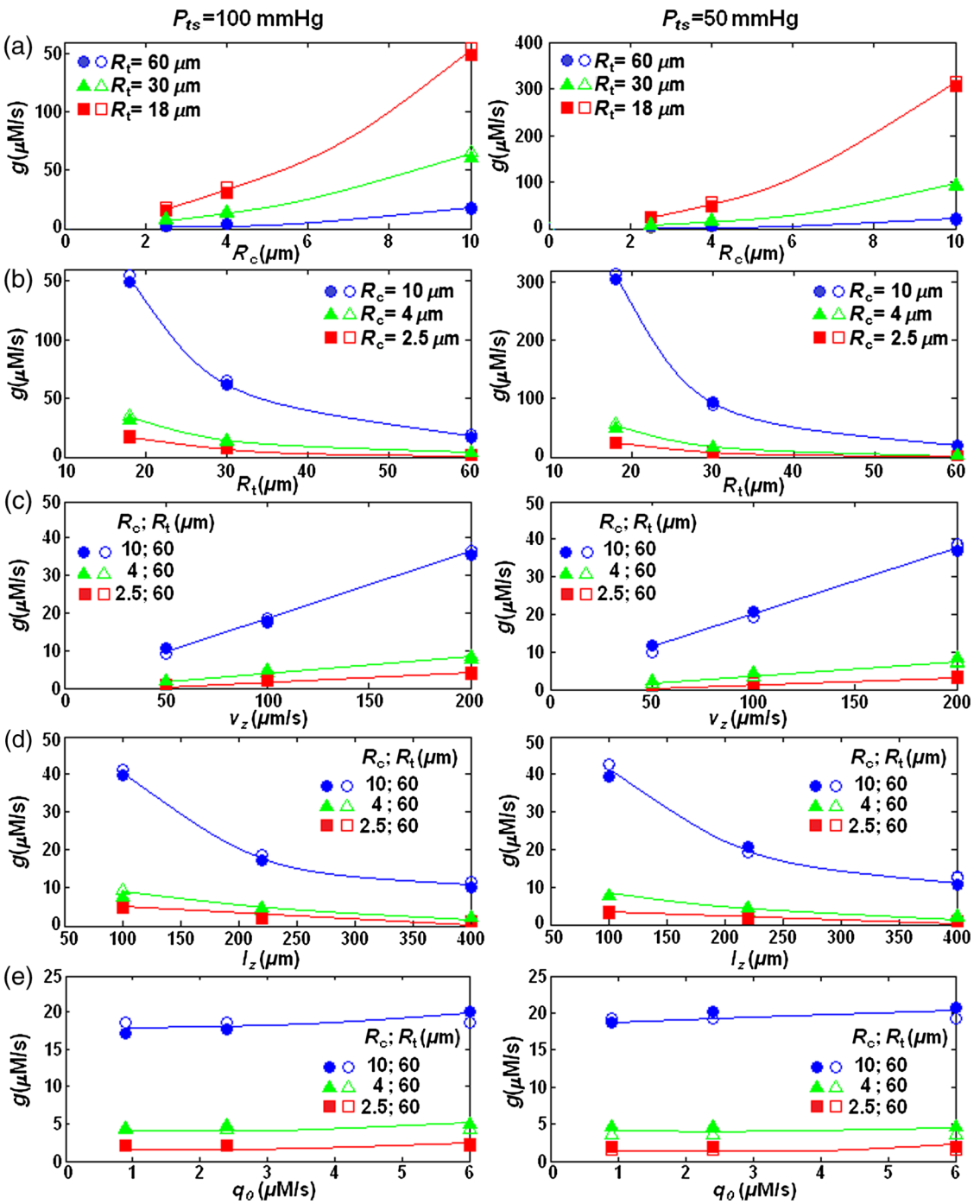

Fig. 6 g versus (a) R_c, (b) R_t, (c) v_z, (d) l_z, and (e) q_0 for $P_{ts} = 100$ mmHg (in the left column) and $P_{ts} = 50$ mmHg (in the right column). The vasculature conditions assumed to have the standard values presented in Table 3. The actual g values (filled-set symbols) are compared with those calculated by using Eqs. (20) and (21) (empty-set symbols). On the basis of the reduced chi-squared ($0.96 \leq \chi^2 \leq 1$), the g values versus R_c, R_t, v_z, and l_z were best fitted with second-order polynomial, second power decay, linear and first power decay curves, respectively.

Oxygen continuously diffuses from the plasma to the tissue (with the volume of $\pi R_t^2 l_z$) where it is consumed. If one assumes that all the capillaries perfusing the tissue are identical and that the oxygen consumption is uniform within the small tissue element shown in Fig. 1(a), then the amount of $^3O_2$ removed from the volume of blood per unit length along the capillary (πR_c^2) is constant. The amounts of oxygen moving across the capillary wall is proportional to that consumed by tissue which is supplied by the capillary:[28]

$$\pi R_c^2 v_z[^3O_2] \propto g\pi R_t^2 l_z = \text{const.} \tag{19}$$

Figures 3 to 5 describing the changes of g with v_z, R_c, R_t, and l_z show close agreement with Fick's principles. While with the same conditions of R_t and R_c, the resulting g values decreased roughly by $1/l_z$, g linearly increased with v_z; g showed a non-linear relationship with R_c, R_t, and q_0. On the basis of the reduced chi-squared ($0.96 \leq \chi^2 \leq 1$), the g values versus R_c [Fig. 6(a)], R_t [Fig. 6(b)], v_z [Figs. 6(c)], and l_z [Figs. 6(d)] were best fitted with a second-order polynomial, second power decay, linear, and first power decay curves, respectively. The fitting equations were used to obtain an empirical Eqs. (20) and (21) that can calculate g directly from v_z, R_c, R_t, l_z, and q_0 for two P_{ts} conditions:

Table 5 The calculated g values using Eqs. (20) and (21) for the same microenvironment ranges examined for the actual g obtained by FEM simulation. The values are presented with the standard deviations obtained from the actual FEM results and the calculated values from Eqs. (20) and (21). The maximum relative (standard) deviation of the fits is 12.82%.

			g (μM/s) calculated from Eqs. (20) and (21)								
			R_c; R_t (μm)								
	v_z (μm/s)	l_z (μm)	2.5;60	4;60	2.5;30	10;60	4;30	2.5;18	4;18	10;30	10;18
	50	220	1.0 ± 0.1	2.1 ± 0.1	3.8 ± 0.2	9.3 ± 0.5	7.5 ± 0.6	9.0 ± 0.5	17.7 ± 0.6	32.6 ± 3.1	77.5 ± 1.9
P_{ts} = 100 mmHg q_0 = 0.9 μM/s	100	220	2.2 ± 0.1	4.2 ± 0.1	7.6 ± 0.4	18.5 ± 0.9	14.9 ± 0.1	18.0 ± 1.7	35.4 ± 4.5	65.3 ± 9.5	155.0 ± 5.6
	200	220	4.3 ± 0.1	8.5 ± 0.4	15.2 ± 2.3	37.1 ± 7.0	29.9 ± 4.8	36.0 ± 7.0	70.9 ± 10.5	130.6 ± 18.7	309.9 ± 21.5
	50	220	1.1 ± 0.1	2.1 ± 0.01	3.8 ± 0.2	9.3 ± 0.9	7.5 ± 0.9	9.0 ± 0.1	17.7 ± 0.5	32.7 ± 2.7	77.5 ± 3.7
P_{ts} = 100 mmHg q_0 = 2.4 μM/s	100	220	2.2 ± 0.1	4.2 ± 0.4	7.6 ± 0.5	18.5 ± 0.6	14.9 ± 0.3	18.0 ± 0.5	35.5 ± 3.0	65.3 ± 3.0	155.1 ± 4.3
	200	220	4.3 ± 0.3	8.5 ± 0.4	15.2 ± 0.9	37.1 ± 0.5	29.9 ± 0.5	36.0 ± 3.1	70.9 ± 11.5	130.7 ± 18.2	310.2 ± 19.4
	50	220	1.1 ± 0.1	2.1 ± 0.1	3.8 ± 0.2	9.3 ± 2.0	7.5 ± 1.2	9.1 ± 0.3	17.9 ± 3.8	32.8 ± 2.1	77.9 ± 8.5
P_{ts} = 100 mmHg q_0 = 6.0 μM/s	100	220	2.2 ± 0.1	4.3 ± 0.4	7.8 ± 1.0	18.6 ± 1.0	15.1 ± 0.6	18.2 ± 0.02	35.7 ± 1.8	65.6 ± 2.2	155.8 ± 0.1
	200	220	4.4 ± 0.1	8.6 ± 0.5	15.3 ± 0.6	37.2 ± 4.4	30.1 ± 2.8	36.4 ± 5.2	71.5 ± 11.1	131.3 ± 15.1	311.5 ± 18.0
	50	220	0.8 ± 0.1	1.8 ± 0.4	3.6 ± 0.5	9.6 ± 0.8	8.2 ± 1.9	12.5 ± 0.1	28.7 ± 2.2	45.1 ± 2.8	157.5 ± 4.1
P_{ts} = 50 mmHg q_0 = 0.9 μM/s	100	220	1.5 ± 0.2	3.5 ± 0.8	7.2 ± 0.7	19.3 ± 0.4	16.4 ± 1.6	25.1 ± 1.5	57.3 ± 9.4	90.1 ± 2.6	315.1 ± 12.4
	200	220	3.1 ± 0.2	7.0 ± 0.7	14.3 ± 0.1	38.5 ± 0.7	32.8 ± 0.9	50.1 ± 1.0	114.6 ± 18.1	180.3 ± 9.3	630.2 ± 20.2
	50	220	0.8 ± 0.1	1.8 ± 0.3	3.6 ± 0.2	9.9 ± 0.6	8.2 ± 2.2	12.6 ± 1.4	28.7 ± 0.9	45.1 ± 4.3	157.6 ± 3.8
P_{ts} = 50 mmHg q_0 = 2.4 μM/s	100	220	1.5 ± 0.3	3.5 ± 0.8	7.2 ± 1.2	19.3 ± 0.8	16.4 ± 1.1	25.1 ± 0.2	57.3 ± 5.9	90.2 ± 2.6	315.2 ± 6.8
	200	220	3.1 ± 0.2	7.0 ± 0.3	14.4 ± 0.6	38.6 ± 0.6	32.8 ± 1.4	50.2 ± 3.2	114.7 ± 18.7	180.4 ± 9.3	630.4 ± 18.2
	50	220	0.8 ± 0.1	1.8 ± 0.4	3.6 ± 0.6	9.7 ± 1.0	8.2 ± 1.7	12.6 ± 1.6	28.8 ± 3.3	45.2 ± 7.5	158.0 ± 2.7
P_{ts} = 50 mmHg q_0 = 6.0 μM/s	100	220	1.6 ± 0.2	3.5 ± 0.8	7.2 ± 0.1	19.3 ± 1.0	16.5 ± 0.4	25.3 ± 0.3	57.6 ± 3.8	90.4 ± 2.8	315.9 ± 6.8
	200	220	3.1 ± 0.3	7.1 ± 1.1	14.5 ± 0.9	38.6 ± 4.9	33.0 ± 1.6	50.5 ± 2.5	115.2 ± 20.4	180.8 ± 8.7	631.8 ± 17.6
	100	100	4.7 ± 0.1	9.3 ± 1.1	16.7 ± 2.6	40.8 ± 2.2	32.9 ± 2.2	39.6 ± 6.3	78.0 ± 1.9	143.8 ± 23.1	341.2 ± 45.1
P_{ts} = 100 mmHg q_0 = 2.4 μM/s	100	220	2.2 ± 0.1	4.2 ± 0.4	7.6 ± 0.5	18.5 ± 0.6	14.9 ± 0.3	18.0 ± 0.5	35.5 ± 3.0	65.3 ± 3.0	155.1 ± 4.3
	100	400	1.2 ± 0.1	2.3 ± 0.1	4.3 ± 0.6	10.2 ± 0.5	8.2 ± 1.7	9.9 ± 0.8	19.5 ± 0.3	35.9 ± 4.1	85.3 ± 2.0
	100	100	3.4 ± 0.2	7.7 ± 0.01	15.8 ± 0.5	42.4 ± 2.5	36.1 ± 0.4	55.2 ± 2.7	126.1 ± 18.8	198.4 ± 27.9	693.4 ± 36.2
P_{ts} = 50 mmHg q_0 = 2.4 μM/s	100	220	1.5 ± 0.3	3.5 ± 0.8	7.2 ± 1.2	19.3 ± 0.8	16.4 ± 1.1	25.1 ± 0.2	57.3 ± 5.9	90.2 ± 2.6	315.2 ± 6.8
	100	400	0.8 ± 0.1	1.9 ± 0.2	4.0 ± 0.1	10.6 ± 0.6	9.0 ± 0.1	13.8 ± 0.4	31.5 ± 0.7	49.6 ± 5.7	173.4 ± 21.8

$$P_{ts}=100\,\text{mmHg}: g[\mu\text{M/s}] = \frac{1200 v_z[\mu\text{m/s}] R_c[\mu\text{m}] \left(R_c[\mu\text{m}] + \left[\frac{100^2+q_0^2[\mu\text{M/s}]}{(50)^2-q_0^2[\mu\text{M/s}]} \right] \right)}{l_z[\mu\text{m}](R_t[\mu\text{m}]+4.2)^2}, \quad (20)$$

$$P_{ts}=50\ \text{mmHg}: g[\mu\text{M/s}] = \frac{1200 v_z[\mu\text{m/s}] R_c[\mu\text{m}] \left(R_c[\mu\text{m}] + \left[\frac{50^2+q_0^2[\mu\text{M/s}]}{(50)^2-q_0^2[\mu\text{M/s}]} \right] \right)}{l_z[\mu\text{m}] \left(R_t[\mu\text{m}] - 4.2 \right)^2}. \quad (21)$$

The relationship between g and q_0 as well as the constant values were obtained and optimized manually based on the relative errors of the actual g and those obtained by Eqs. (20) and (21). For the range of microenvironments shown in Table 3, Eqs. (20) and (21) determine g values in the ranges of 0.6 to 685.3 μM/s for $P_{ts}=100$ mmHg and 0.4 to 1390 μM/s for $P_{ts}=50$ mmHg. The maximum g value of 1390 μM/s is obtained for $R_c=10$ μm, $R_t=18$ μm, $v_z=200$ μm/s, $P_{ts}=50$ mmHg, $q_0=6$ μM/s, and $l_z=100$ μm. The minimum g value of 0.4 μM/s is calculated for $R_c=2.5$ μm, $R_t=60$ μm, $v_z=50$ μm/s, $P_{ts}=50$ mmHg, $q_0=0.9$ μM/s, and $l_z=400$ μm. Table 5 shows the results of Eqs. (20) and (21) for the physiological parameters listed in Table 3. The g values are presented with the standard deviations obtained from the actual FEM results and the calculated values from Eqs. (20) and (21). The relative errors were also measured as the percentages of the deviations divided by the FEM calculated g values. The maximum error of 27% occurs for the blood vessel with $P_{ts}=100$ mmHg, $q_0=0.9$ μM/s, $v_z=200$ μm/s, $l_z=220$ μm, $R_c=2.5$ μm, and $R_t=18$ μm; the minimum error of 0.03% occurs for the blood vessel with $P_{ts}=100$ mmHg, $q_0=6$ μM/s, $v_z=100$ μm/s, $l_z=220$ μm, $R_c=10$ μm and $R_t=18$ μm.

4 Conclusion

The accurate estimation of the maximum oxygen supply rate, g, is very important for the mathematical investigation of complex PDT mechanisms. In this study, we suggested a simplified expression for g that can replace the complex modeling of blood vasculature while maintaining reasonable accuracy. Using the microscopic model, the relationship of the oxygen supply rates versus $[^3O_2]/[^3O_2]_0$ has been examined for Photofrin-mediated PDT treated at ϕ ranging from 25 to 150 mW/cm^2; the slope of the linear fit to these data represents the g value in μM/s. The simulations have been also tested for different photochemical parameters corresponding to mTHPC-, BPD-, and HPPH-mediated PDT. The obtained results showed a linear relationship independent of ϕ, ξ, σ, and β. The possible g values in Photofrin-mediated PDT were then calculated for a broad range of physiological parameters that have been measured in the past for normal and tumor vasculatures. Examination reveals that the g values can range from 0.4 to 1390 μM/s depending on the actual physiological environment. The maximum g value of 1390 μM/s was obtained for blood vessels with $R_c=10$ μm, $R_t=18$ μm, $v_z=200$ μm/s, $P_{ts}=50$ mmHg, $q_0=6$ μM/s, and $l_z=100$ μm. The minimum g value of 0.41 μM/s was calculated for $R_c=2.5$ μm, $R_t=60$ μm, $v_z=50$ μm/s, $P_{ts}=50$ mmHg, $q_0=0.9$ μM/s, and $l_z=400$ μm.

Based on Fick's principle,[28] if all the capillaries perfusing the tissue are identical and the oxygen consumption is uniform within the tissue element, the amount of oxygen moving across the capillary wall is proportional to that consumed by tissue which is supplied by the capillary ($v_z\pi R_c^2[^3O_2] \propto g\pi R_t^2 l_z$). This is in close agreement with our simulation outcome which estimates g to increase with decreasing l_z (first power decay) and R_t (second power decay) and increasing R_c (quadratic second-order polynomial enhancement), and v_z (linear enhancement). Our model also anticipates g to increase nonlinearly and slowly with q_0.

A comparison of our estimated g values with those obtained by the previous *in vivo* studies shows that our calculation is accurate and the g value can be potentially used for our macroscopic model [Eqs. (1–5)].

Acknowledgments

We thank the useful discussions with Dr. Jarod C. Finlay on the theory. This research was supported by the National Institute of Health (NIH R01 CA 154562).

References

1. T. J. Dougherty et al., "Photodynamic therapy," *J. NCI.* **90**(12), 889–905 (1998).
2. M. J. Niedre et al., "*In-vitro* tests of the validity of singlet oxygen luminescence measurements as a dose metric in photodynamic therapy," *Cancer Res.* **63**(22), 7986–7994 (2003).
3. M. J. Niedre et al., "Singlet oxygen luminescence as an *in vivo* photodynamic therapy dose metric: validation in normal mouse skin with topic amino-levulinic acid," *Brit. J. Cancer* **92**(2), 298–304 (2005).
4. M. T. Jarvi et al., "Singlet oxygen luminescence dosimetry (SOLD) for photodynamic therapy: current status, challenges and future prospects," *Photochem. Photobiol.* **82**, 1198–1210 (2006).
5. M. J. Niedre, M. S. Patterson, and B. C. Wilson, "Direct near-infrared luminescence detection of singlet oxygen generated by photodynamic therapy in cells *in vitro* and tissues *in vivo*," *Photochem. Photobiol.* **75**, 382–391 (2002).
6. D. J. Robinson et al., "Fluorescence photobleaching of ALA-induced protoporphyrin IX during photodynamic therapy of normal hairless mouse skin: the effect of light dose and irradiance and the resulting biological effect," *Photochem. Photobiol.* **67**, 140–149 (1998).
7. T. K. Lee and T. H. Foster, "Integrated spectroscopy and PDT delivery for various treatment geometries," in *Frontiers in Optics 2008/Laser Science XXIV/Plasmonics and Metamaterials/Optical Fabrication and Testing*, Optical Society of America, Rochester, New York (2008).
8. T. H. Foster et al., "Intratumor administration of the photosensitizer pc 4 affords photodynamic therapy efficacy and selectivity at short drug-light intervals," *Transl. Oncol.* **3**(2), 135–41 (2010).
9. S. Mitra and T. H. Foster, "*In vivo* confocal fluorescence imaging of the intratumor distribution of the photosensitizer mono-L-aspartylchlorin-e6," *Neoplasia.* **10**(5), 429–438 (2008).
10. M. Seshadri et al., "Light delivery over extended time periods enhances the effectiveness of photodynamic therapy," *Clin. Cancer Res.* **14**(9), 2796–805 (2008).
11. R. Cheung et al., "Correlation of *in vivo* photosensitizer fluorescence and photodynamic-therapy-induced depth of necrosis in a murine tumor model," *J. Biomed. Opt.* **8**(2), 248–252 (2003).
12. T. M. Busch et al., "Increasing damage to tumor blood vessels during motexafin lutetium-PDT through use of low fluence rate," *Radiat. Res.* **174**(3), 331–40 (2010).
13. K. K.-H. Wang et al., "Explicit dosimetry for photodynamic therapy: macroscopic singlet oxygen modeling," *J. Biophoton.* **3**(5–6), 304–318 (2010).

14. J. S. Dysart and M. S. Patterson, "Characterization of Photofrin photobleaching for singlet oxygen dose estimation during photodynamic therapy of MLL cells *in vitro*," *Phys. Med. Biol.* **50**, 2597–2616 (2005).
15. J. C. Finlay et al., "Photobleaching kinetics of Photofrin *in vivo* and in multicell tumour spheroids indicate two simultaneous bleaching mechanisms," *Phys. Med. Biol.* **49**, 4837–60 (2004).
16. T. C. Zhu et al., "Macroscopic modeling of the singlet oxygen production during PDT," *Proc. SPIE* **6427**, 1–12 (2007).
17. B. Liu, T. J. Farrell, and M. S. Patterson, "A dynamic model for ALA-PDT of skin: simulation of temporal and spatial distributions of ground-state oxygen, photosensitizer and singlet oxygen," *Phys. Med. Biol.* **55**, 5913–5932 (2010).
18. T. C. Zhu et al., "Comparison of singlet oxygen threshold dose for PDT," *Proc. SPIE* **8931**, 89310I (2014).
19. J. P. Whiteley, D. J. Gavaghan, and C. E. W. Hahn, "Mathematical modeling of oxygen transport to tissue," *J. Math. Biol.* **44**, 503–522 (2002).
20. M. P. Wiedeman, "Dimensions of blood vessels from distributing artery to collecting vein," *Circ. Res.* **12**, 375–378 (1963).
21. J. W. Baish et al., "Scaling rules for diffusive drug delivery in tumor and normal tissues," *Proc. Natl. Acad. Sci.* **108**, 1799–1803 (2011).
22. S. Lauk et al., "Comparative morphometric study of tumor vasculature in human squamous cell carcinomas and their xenotransplants in athymic nude mice," *Cancer Res.* **49**(16), 4557–4561 (1989).
23. J. D. Murray, "On the molecular mechanism of facilitated oxygen diffusion by haemoglobin and myoglobin," *Proc. Roy. Soc. Lond. B.* **178**, 95–110 (1971).
24. K. K. Wang, S. Mitra, and T. H. Foster, "A comprehensive mathematical model of microscopic dose deposition in photodynamic therapy," *Med. Phys.* **34**, 282–293 (2007).
25. A. Carreau et al., "Why is the partial oxygen pressure of human tissues a crucial parameter? Small molecules and hypoxia," *J. Cell. Mol. Med.* **15**, 1239–1253 (2011).
26. H. Chaplin, P. L. Mollison, and H. Vetter, "The body/venous hematocrit ratio: Its constancy over a wide hematocrit range," *J. Clin. Invest.* **32**(12), 1309–1316 (1953).
27. A. J. Williams, "Assessing and interpreting arterial blood gases and acid-base balance," *Brit. Med. J.* **317**, 1213–1216 (1998).
28. R. N. Pittman, *Regulation of Tissue Oxygenation*, Morgan & Claypool Life Sciences, San Rafael, California (2011).

Timothy C. Zhu received his PhD degree in 1991 in physics from Brown University. He is currently a professor in the Department of Radiation Oncology at the University of Pennsylvania. His current research interests include explicit PDT dosimetry, singlet oxygen explicit dosimetry (SOED), integrated system for interstitial and intracavitory PDT, diffuse optical tomography, *in vivo* dosimetry, and external beam radiation transport.

BaochangLiu received his PhD degree in medical physics in 2012 from McMaster University, where he specialized in photodynamic therapy (PDT) dosimetry. He continued his research as a postdoctoral fellow in the Department of Radiation Oncology at the University of Pennsylvania. His research interests include modeling PDT dosimetry and oxygen transport in tissue, *in vivo* explicit dosimetry for interstitial PDT, developing direct $^1O_2$ dosimetry system, and tissue optics.

RozhinPenjweini received her PhD degree in 2012 in physics from the University of Vienna. She is currently a postdoctoral researcher in the Department of Radiation Oncology at the University of Pennsylvania. Her current research interest is *in vivo* explicit PDT and singlet oxygen dosimetry. She also has practical experience in various fluorescence microscopy techniques for studying the structure, transport, and stability of nanomedicines for PDT treatment of cancer.